Nuclear Magnetic Resonance and Restrained Molecular Dynamics Studies of the Interaction of an Epidermal Growth Factor-Derived Peptide with Protein Tyrosine Phosphatase 1B[†,‡]

Nicholas R. Glover[§] and Alan S. Tracey*

Department of Chemistry and Institute of Molecular Biology and Biochemistry, Simon Fraser University, Burnaby, British Columbia V5A 1S6, Canada

Received October 23, 1998; Revised Manuscript Received February 8, 1999

ABSTRACT: The epidermal growth factor-derived (EGFR988) fluorophosphonate peptide, DADE(F_2Pmp)-L, is a potent (30 pM) inhibitor of the protein tyrosine phosphatase PTP1B. Nuclear magnetic resonance (NMR) transferred nuclear Overhauser effect (nOe) experiments have been used to determine the conformation of DADE(F_2Pmp)L while bound in the active site of PTP1B. When bound, the peptide adopts an extended β-strand conformation. Molecular modeling and molecular dynamics simulations allowed the elucidation of the sources of many of the interactions leading to binding of this inhibitor. Electrostatic, hydrophobic, and hydrogen-bonding interactions were all found to contribute significantly to its binding. However, despite the overall tight binding of this inhibitor, the N-terminal and adjacent residue of the peptide were virtually unrestrained in their motion. The major contributions to binding arose from hydrophobic interactions at the leucine and at the aromatic center, hydrogen bonding to the *pro-R* fluorine of the fluorophosphonomethyl group, and electrostatic interactions involving the carboxylate functionalities of the aspartate and glutamate residues. These latter two residues were found to form tight contacts with surface recognition elements (arginine and lysine) situated near the active-site cleft.

The protein tyrosine phosphatases (PTPases)[1] consist of a ubiquitous assortment of enzymes that are crucial to the regulation of cell function. These enzymes function via down-regulation of tyrosine kinase activity, a function expressed by dephosphorylation of the phosphotyrosine of the active kinase. They are crucial for many cellular functions such as cell mitosis, T-cell activation, and growth factor and insulin receptor signaling (*1*−*4*). Because of their wide-ranging function, PTPases are attracting increasing attention as potential targets for enzyme-specific drugs; for instance, for the treatment of autoimmune diseases, arthritis, cancer, and diabetes.

Our initial interest in PTPases arose from our studies of the role of vanadate and its complexes as activators or inhibitors of the function of enzymes that normally metabolize phosphate-containing substrates (*5*−*7*). This interest has been fueled by the knowledge that vanadium and a number of vanadium complexes are insulin-mimetic in animals (*8*−*10*). This suggests that there may be a connection between vanadium and the action of the insulin receptor. It is possible that vanadate might activate the insulin receptor kinase activity (*11*) but it is well-known to be a potent nonselective inhibitor of PTPase activity. An important property of a viable pharmaceutical agent is that it targets a specific enzyme. Obviously vanadate fails in this regard, but if complexes of vanadium are active (as opposed to simply being transport agents for vanadium) as insulin mimetics, then it may be possible to build in selectivity by suitably modifying the liganding groups of the complex. In this regard, we are interested in the development of selective vanadate-based inhibitors of the protein tyrosine phosphatases PTP1B and CD45.

We have chosen to approach this problem of selectivity by first initiating structural studies of known peptide-based inhibitors of PTP1B (*12*, *13*). Like the other PTPases, PTP1B is quite nonselective toward small phosphotyrosine substrates. This is not surprising because there is a high degree of structural homology between the active sites of the known PTPases (*3*, *14*, *15*). To build in selectivity of inhibition, it therefore is imperative that the inhibitor reaches out to recognition elements that are removed from the active-site pocket. PTP1B is one of the best known of the PTPases and there is evidence available that suggests this PTPase is a regulator of the insulin receptor function (*16*, *17*). This PTPase offers a marked advantage over study of other systems in that it has been structurally characterized from X-ray studies. In particular, the structure of a mutant form,

[†] Thanks are gratefully extended to the Merck Frosst Centre for Therapeutic Research for its financial support of this work.

[‡] This material was abstracted, in part, from the Ph.D. thesis of N.R.G.

[§] Present address: University Medical Discoveries Inc., 100 International Blvd., Toronto, Ontario M9W 6J6, Canada.

[1] Abbreviations: EGFR, epidermal growth factor receptor; IRK, insulin receptor kinase; PTPase, protein tyrosine phosphatase; PTP1B, protein tyrosine phosphatase 1B; GST, glutathione S-transferase; EDA, ethylenediamine; BMS, bis(mercaptoethyl)sulfone; DTT, dithiothreitol; F_2Pmp, (difluorophosphonomethyl)phenylalanine; nOe, nuclear Overhauser effect; COSY, correlation spectroscopy; DQF−COSY, double quantum filtered correlation spectroscopy; TOCSY, total correlation spectroscopy; NOESY, nuclear Overhauser effect enhancement spectroscopy; ROESY, rotating-frame nuclear Overhauser effect enhancement spectroscopy.

10.1021/bi9825450 CCC: $18.00
Published on Web 04/02/1999

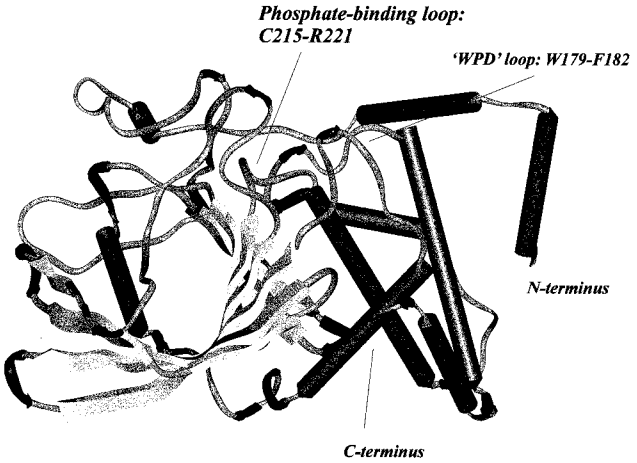

FIGURE 1: Representation of the secondary structure of PTP1B. PTP1B consists of a highly curved, eight-stranded mixed β-sheet surrounded by two α-helices on one side and five on the other. The relative positions of various loops and residues are indicated. The secondary structure is represented according to the formalism of Kabsch and Sanders (*98*). Key: α-helices, large tubes; β-sheet, wide ribbon; loop, narrow gray ribbon; turn, narrow black arrow.

where the essential active-site cysteine has been replaced by a serine, has been determined in which a phosphotyrosine oligopeptide substrate [an epidermal growth factor receptor peptide, EGFR988, of sequence DADE(pY)L] is bound in the active site (*18*). A representation of the structure of PTP1B is provided in Figure 1.

In the present study, nuclear magnetic resonance (NMR) spectroscopy has been utilized to structurally characterize an EGFR988 (difluorophosphonomethyl)phenylalanine analogue of the above peptide [sequence DADE(F_2Pmp)L] by use of the mutual nuclear Overhauser effect (nOe) enhancement between the protons of the peptide inhibitor that is induced by binding of the peptide in the active site of PTP1B. In this case, a transferred nOe enhancement was measured since the peptide was in sufficiently rapid exchange. DADE(F_2Pmp)L, with an IC_{50} of 0.03 μM, is one of the most potent inhibitors of PTP1B that has been reported. The nOe values were used in a constrained distance geometry algorithm to obtain an ensemble of different but structurally similar peptide conformations. The ensemble of structures was then subjected to a docking protocol that ranked the structures with regard to their complementarity with the active site. Subsequent energy minimization and simulated dynamics calculations allowed various modes of interaction with PTP1B to be examined.

MATERIALS AND METHODS

Structural Experiments

Peptide and Protein. GST−PTP1B and DADE(F_2Pmp)L (EGFR988) were kindly provided by Merck Frosst Centre for Therapeutic Research, Montreal. The N-terminal domain of PTP1B as provided (residues 1−298) was expressed as a glutathione S-transferase fusion protein, GST−PTP1B, in *Escherichia coli* (*19*). Protein concentrations either were assayed according to the method of Bradford (*20*) or were measured by UV spectroscopy at 280 nm (*19*, *21*). The purity of the protein samples was established by SDS−PAGE. The activity of the protein samples was assayed prior to the NMR experiments according to the established procedure (*19*, *22*). The purity of DADE(F_2Pmp)L was confirmed by ^{1}H NMR spectroscopy.

From the molecular mass of the protein (~75 kDa), it can be estimated (*23*) from a calculated correlation time (*24*) of 30 ns that a protein-to-peptide ratio of about 1:10 will give optimum nOe enhancements. Solutions for transferred nOe experiments were therefore prepared with a final peptide concentration of ~2 mM and a GST−PTP1B/peptide ratio of about 1:10. The pH of each protein/peptide solution was adjusted in order to provide the best resolution between individual spin systems of the peptide, while the pH of the solution was maintained within the optimum catalytic range of the enzyme (pH ~6.0−7.0) (*15*). The appropriateness of the predicted experimental conditions was verified by control experiments in which the peptide-to-protein ratio, solution temperature, and pH were varied.

NMR Sample Preparation. All samples for NMR spectroscopy were prepared as aqueous solutions in a buffer containing 2 mM EDA or 2 mM phosphate, pH ~6.5−7.0, 0.20 M NaCl, 0.1 mM bis(mercaptoethyl)sulfone (BMS) or 0.1 mM dithiothreitol (DTT), and 5% D_2O/95% H_2O. Samples of the free peptides were prepared as 2 mM solutions. The pH of each peptide solution was adjusted to an appropriate value by adding a small amount of either HCl or NaOH (uncorrected for the deuterium isotope effect). The pH of the samples were measured directly in the NMR tube with a glass electrode (Bradley James Inc.) and calibrated against standard buffers at pH 4.0 and 7.0. Samples of the peptides in the presence of GST−PTP1B were prepared by titrating an aliquot of the protein into a stock solution of the peptide at the appropriate pH. All samples were filtered into the NMR tube through a Celite over glass wool plug, filled with nitrogen gas, and sealed. All chemicals used in the study were reagent-grade or better.

NMR Experiments. Nuclear magnetic resonance experiments were carried out on a Bruker AMX600 spectrometer operating at a ^{1}H frequency of 600.13 MHz with a nonspinning sample. All two-dimensional experiments were recorded in phase-sensitive mode (TPPI) (*25*). The spectral width in both dimensions was 7240−8196 Hz, with the carrier frequency set at the water resonance. Except where noted, water suppression was achieved by the WATERGATE gradient-echo method with a 3−9−19 pulse sequence (*26*). NOESY experiments (*27*) were performed on the free peptides at 298 K with typical mixing times of 50, 100, 150, 300, and 600 ms. Transferred nOe experiments of the peptide/protein complexes were carried out with the standard NOESY pulse sequence at 298 K (*27*). Spectra were recorded at a series of mixing times, typically 25, 50, 75, 100, 150, 300, and 600 ms. ROESY and transferred ROESY experiments were performed at 298 K with spin-lock fields of 100−300 ms duration (*28*, *29*). Water suppression during the ROESY experiments was achieved by continuous low-power presaturation (2 s) during the relaxation delay, with the transmitter frequency set on the H_2O resonance (*30*). Sequence-specific assignments of peptide resonances were established by analysis of the cross-peak patterns of transferred NOESY spectra and TOCSY spectra (*31*, *32*). The latter were acquired with a spin-locked MLEV-17 sequence (150 ms). Assignments were confirmed with DQF−COSY (double quantum filtered correlation spectroscopy) experiments (*33*, *34*). The spectra were obtained with presaturation

(2 s) during the recycling delay (*30*). The majority of the spectra were collected as 512 t_1 values with 40−128 scans/increment, each with 2K complex data points in t_2 and a relaxation delay of 1−2 s (total experimental time ∼10−22 h/experiment). The data were processed either directly on the AMX600 spectrometer using the standard UXNMR software (Bruker) or off-line on a SGI Indigo2 workstation using XWIN NMR (Bruker) or FELIX software (*35*). Data sets were apodized in both directions by either a 30−60° shifted squared sine-bell or a Lorentzian to Gaussian transformation function. Data sets were zero-filled to 1−2K in the t_1 dimension. Following Fourier transformation and phase correction, a polynomial fifth-order function was used for baseline correction in both dimensions prior to volume integration. All chemical shifts were referenced to an external sample of DSS at 0.0 ppm.

Derivation of Distance Restraints. The nOe distance restraints were determined by use of the FELIX program (*35*). Distance restraints were derived from volume integration of a rectangular box defined around each cross-peak on the 100 ms mixing time of the representative transferred NOESY spectrum recorded at 298 K. Transferred nOe cross-peak intensities were classified as strong, medium, weak, or very weak by analyzing one-dimensional *F*1 and *F*2 slices from selected NOESY spectral regions, as well as according to volume integration. A known fixed distance (*o*-phenyl protons, 2.5 Å) was used for internal calibration purposes. Provisional distance cutoffs were then assigned: strong nOes, 1.8−2.8 Å; medium nOes, 1.8−3.3 Å; weak nOes, 1.8−4.0 Å; very weak nOes, 1.8−5.0 Å. Distance assignments were confirmed from analyses of nOe intensity build-up curves and by counting NOESY cross-peak contours. The upper bounds of restraints involving nonresolvable methylene or methyl protons were adjusted according to the literature (*36*). Free ligand cross-peak intensities were small compared to those of transferred nOe cross-peak intensities from the bound ligand and no correction for free ligand nOes was necessary in the derivation of the distance restraints.

Structural Calculations. All structural calculations were performed on a Silicon Graphics (SGI) Indigo II workstation. Peptide sequences were computationally built with the BIOPOLYMER molecule of INSIGHT_II (*35*). To ensure that the starting geometries of the peptides were correct, the structures were first minimized in the absence of nOe restraints by the program DISCOVER (*37*). Steepest descent minimization (100 steps) was followed by 1000 steps of minimization by conjugate gradients. A variable-target function distance geometry program [DGII in INSIGHT_II (*35*)] was used for the structural calculations based upon the NMR-derived distance restraints (*38*). In the absence of stereospecific assignments, pseudoatom corrections were used in these calculations (*36*). A conjugate gradient method was used to minimize the full-matrix error function. At the final stage of refinement, *in vacuo* molecular dynamics (50 ps) and energy minimization were used to relieve structural irregularities (e.g., bad contacts, bad bond lengths) and to improve structures. The resulting conformers were analyzed and compared by use of INSIGHT_II (*35*). Upon completion of the calculations, nOe restraints with distance violations greater than 0.1 Å were listed and examined. In cases where there was uncertainty in volume integrals because of spectral overlap, distance bounds were relaxed to those of the upper class (e.g., from the 3.3 Å class to the 4.0 Å class). When no further improvements were achieved after iterative refinement of the distance restraints (typically 2−3 sets of calculations), 500 allowed structures were calculated in a final run.

Transferred nOe Simulations. Simulation of nOes were performed with the program CORCEMA (*39*), which accounted for spin diffusion effects mediated both through protons on the ligand and via protons on the protein. Transferred nOe simulations were carried out as follows: A tumbling correlation time for the oligopeptide−PTP1B complexes was estimated to be ∼30 ns, as expected for a globular protein of molecular mass ∼75 kDa (*24*). A short correlation time of 0.4 ns was assumed for the free peptides. The internal dynamics of the peptide methyl groups were treated with a three-site jump model with a correlation time of 2 ps. The simulation utilized a magnetization leakage rate of 0.2 s^{-1} for the free peptide and 2 s^{-1} for the peptide−protein complex. The dissociation constant for the peptide−protein complex, K_d, and the value of k_{off} were estimated on the basis of the IC_{50} of each peptide. The mixing times and the relaxation delay were set to those values used in the transferred nOe experiments. The resulting nOe volume matrixes determined from nOe simulations were compared to the experimental volumes.

Rational Conformational Sampling. The Connolly molecular surface (MS) algorithm as integrated within the DOCK package was used to generate a molecular surface encompassing the entire active site of PTP1B (density of 5.4 points/$Å^2$; 1.4 Å radius probe sphere) (*40*, *41*). The surface was converted into spheres by use of the SPHGEN module of DOCK (*42*, *43*). The scoring grids were constructed with the DOCK modules DISTMAP and CHEMGRID for contact and force field scoring, respectively. Scoring/matching was performed with DOCK version 3.5 (*44*). Matching parameters used in the calculations were as follows: receptor bin width/overlap, 1.0, 0.2; ligand bin width/overlap, 1.0, 0.2; matching tolerance, 1.5. Rigid-body minimization (500 iterations) and degeneracy checking were employed for refinement purposes (*44*). Color matching was applied to the peptide termini and to the active-site binding pocket (each of opposite colors to prevent matching) (*44*). The set of 500 conformers derived from the transferred nOe measurements were converted into a structural database and scored against the contact grid according to favorability of geometric and force field fit. This process facilitated the ranking of conformers according to the most favorable match to both the shape and energetic requirements of the active site of PTP1B.

Molecular Modeling

Preparation. Heavy-atom coordinates of the catalytically inactive Cys215Ser mutant of PTP1B were extracted from the X-ray crystallographic data obtained for the liganded PTP1B complex (*18*). The side chain of S215 was replaced with cysteine in its reduced thiolate form (*15*). Structures of the enzyme−ligand complexes were calculated, displayed, and manipulated with the INSIGHT_II program (*35*) running on a Silicon Graphics O2 R5000 workstation. Hydrogen atoms were added to the heavy atoms of the protein according to a pH of 7 with the BUILDER module of INSIGHT_II.

Glutamic acids, aspartic acids, lysines, and arginines were modeled as charged side chains; histidine was neutral with the hydrogen at Ne. Crystallographically observed water molecules were retained in the model. To reduce any bad atom−atom van der Waals clashes resulting from crystal close contacts, the initial protein model was initially minimized with 2500 steps of steepest descent minimization, followed by further minimization by conjugate gradients until the maximum derivative of the system was <0.01 kcal/Å (*45*, *46*). As described above, peptide conformers were obtained from distance geometry calculations and were docked into the catalytic site of PTP1B by use of the program DOCK (*47*).

Since the methine carbon of the side chain of the (difluorophosphonomethyl)phenylalanine (F_2Pmp) has no protons, it was not possible to define the orientations of the side chain from the ^{1}H transferred nOe experiments. Consequently, following peptide docking, the side chain of F_2-Pmp was manually positioned within the PTP1B binding pocket according to the most energetically favorable orientation. This was determined by monitoring the change in intermolecular peptide−protein interaction energy ensuing from rotation about the χ_1 torsion angle of F_2Pmp by use of the DOCKING module of INSIGHT_II (*35*). The peptide−protein complex was constrained during these calculations. A similar methodology has been applied to position steroidal substrates in the active site of cytochrome P450 (*48*). Following this protocol, it was found that the most energetically favorable orientation of the (difluorophosphonomethyl)-phenylalanine headgroup placed this functionality in the general position occupied by the phosphotyrosine side chain of pTyr in the liganded X-ray crystal structure (*18*).

All dynamics calculations were carried out with a hydrated structural model. The DADE(F_2Pmp) and surrounding areas of the peptide−PTP1B complexes was surrounded by a 15 Å radius inner semisphere of water that, in turn, was contained within a 10 Å thick inner layer of water. This created a solvent cage encompassing the bound peptide in its complex with PTP1B. This solvent cage was constrained by an outer 5 Å deep layer of water that was restrained in order to prevent its evaporation during the calculations. Overlapping water molecules and water molecules whose oxygens were within 2.8 Å of any protein atom were deleted. This led to a system comprising ∼1000−1500 water molecules. The solvent employed in these modeling studies was represented by the consistent valence force field (CVFF) water model (*49*). Control simulations confirmed that the effects of restraining the outer layer of water did not significantly influence the energy or dynamical motion of the peptides within the active site.

Force Field. Formal and partial charges on the ligand−protein complexes were calculated with the CVFF (*49*−*52*). Electrostatic interactions were represented by a distance-dependent dielectric. Double cutoffs of 15 and 13 Å were applied in these calculations; no spline switching function was used. The CVFF force field intrinsically accounts for hydrogen bonding as a consequence of standard van der Waals and electrostatic parameters (*50*−*52*).

Energy Minimization. Prior to the molecular dynamics simulations, the solvated peptide−protein complexes were first minimized to convergence. Interaction energies were then calculated for the fully minimized systems. To make the computations tractable, calculations were restricted to those residues within 12 Å of the docked peptide ("active site"). The following minimization protocol was employed:

(1) The hydrogen atoms of the entire solvent shell were initially minimized to 1.0 kcal/Å convergence by 1000 steps of steepest descents and were then minimized further to 0.1 kcal/Å convergence by 5000 cycles of conjugate gradients. All of the enzyme and peptide residues and the oxygen atoms of the water molecules were kept fixed. No Morse potentials or cross terms were included.

(2) All of the solvent atoms were minimized to 1.0 kcal/Å convergence by 1000 steps of steepest descents and were further minimized to 0.1 kcal/Å by 5000 cycles of conjugate gradients. Again, all of the enzyme and peptide residues were kept fixed. No Morse potentials or cross terms were included.

(3) Full minimization of the system was performed in three stages. First, 10 000 cycles of steepest descents minimization were performed to 0.1 kcal/Å convergence with Morse potentials and cross terms turned off. This was followed by 10000 steps of steepest descents minimization to 0.1 kcal/Å, with Morse potentials and cross terms applied to the system. Third, 25 000 iterations of conjugate gradients were performed with Morse potentials and cross terms to a convergence of 0.0001 kcal/Å. The backbone atoms of PTP1B active-site residues were restrained during these calculations while the side chains were free to move. At this stage, all of the remaining enzyme residues were fixed. The peptides were free to move during the full minimization procedure. Restraints in the form of the nOe distance ranges were applied to the peptides throughout the minimization. The inner shell and the inner layer of solvent molecules were unrestrained at this stage, while the outer layer of solvent was fixed in place.

Molecular Dynamics. Following energy minimization, molecular dynamics (MD) simulations were performed with the program DISCOVER (*35*). The side chains of PTP1B active site residues were unrestrained during molecular dynamics, while the backbone atoms either were fully restrained or were tethered with a harmonic restraining function of 500.0 kcal/Å. MD integrations were performed with the Verlet leapfrog algorithm with a time step of 1 fs (*46*, *53*). A constant temperature was maintained during the course of the simulation by weakly coupling the system to a thermal bath (*54*). Initial velocities were obtained from a Maxwellian distribution (*46*). The system was slowly warmed from 0 to 300 K and the equilibrated for 20 ps of dynamics simulations. Molecular dynamics simulations were then continued for an additional 100 ps of production dynamics (*55*). During these production simulations, molecular trajectories were recorded every picosecond.

MD Analysis. Time-dependent peptide−protein interactions were evaluated in four ways: (1) Root-mean-square deviations (RMSD) from initial docked orientations were determined to assist in identification of major peptide and protein motion as a function of time. (2) Distances for important hydrogen bonds were monitored during the course of the MD simulations. (3) The ANALYSIS module of INSIGHT_II (*35*) was used to examine time-dependent fluctuations in energy terms, distances, and torsion angles during the trajectory. (4) Deviations from the distance restraints were monitored at periodic intervals.

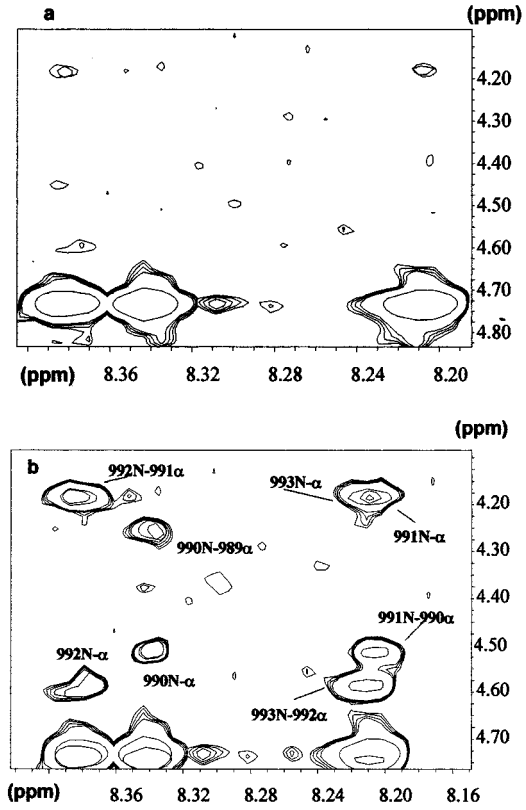

FIGURE 2: NH−CHα region of the nOe spectrum of DADE(F_2-Pmp)L. Spectrum obtained in the absence (a) or presence (b) of 0.2 mM GST−PTP1B. In panel b, protons are designated by the attached carbon or nitrogen of the numbered residue. Various intraresidue and sequential transferred nOe cross-peaks are indicated. Conditions of the experiments: concentration of DADE(F_2-Pmp)L 2 mM; pH 6.5; temperature 298 K; nOe mixing time 150 ms.

Surface Area Calculations. Surface areas were calculated according to the method of Lee and Richards (*56*) and were calculated with a 1.4 Å radius probe as implemented in the computer program NACCESS (*57*).

Additional Simulations. By a similar procedure to that outlined above, computations were also performed for the following systems: (1) Free peptide conformers in solvated shells; (2) peptide−PTP1B complexes *in vacuo*; (3) peptide−PTP1B complexes with a fully unrestricted active site; (4) peptide−PTP1B complexes with sTyr/F_2Pmp side chain in alternative modes; (5) unligated PTP1B in closed and open-loop configurations, *in vacuo* and solvated; and (6) Crystallographic complex of DADE(pY)L-PTP1B in a solvated shell.

RESULTS

Free Peptide. The 1D proton NMR spectrum of the EGFR988-derived peptide, DADE(F_2Pmp), is well-resolved with both the amido N−H protons and the aromatic and aliphatic protons providing sharp signals. To assign the subspectra of the various amino acid residues, both DQF−COSY and TOCSY spectra were obtained. This did not provide sufficient information for the sequence-specific assignment of the two aspartate residues. Also, the NOESY spectra of the free peptide (Figure 2a) provided only a few very weak $NH_i/CH_{\alpha i}$ nOe cross-peaks. These were insufficient to sequence the peptide. This lack of NOESY interresidue correlations suggested the peptide adopted a dynamic unstructured form in solution. Support for this possibility was obtained from a rotating-frame nOe (ROESY) spectrum. As was found for the NOESY spectra, the intranuclear correlations were very weak. It was therefore concluded that the free peptide in aqueous solution is not structured but in rapid dynamic equilibrium between various random coil structural elements.

Table 1: Proton Chemical Shifts for DADE(F_2Pmp)L[a] in H_2O/D_2O (9:1),[b] pH 6.5 and 298 K

residue	HN	CHα	CHβ	CHγ	others
Asp988		4.60	2.80		
Ala989	8.70	4.28	1.10		
Asp990	8.34	4.55	2.60		
			2.70		
Glu991	8.21	4.20	1.90	2.00	
				2.19	
F_2PmpL992	8.38	4.61	3.19		$CH_2\delta$ 7.51
			3.17		$CH_2\epsilon$ 7.34
Leu993	8.22	4.20	1.59	1.59	$CH_3\delta$ 0.99,0.81

[a] In the absence of GST−PTP1B. [b] Chemical shifts in parts per million are referenced relative to external DSS (0.00 ppm).

Bound Peptide. Figure 2b shows a partial transferred NOESY spectrum obtained under conditions similar to those of the free peptide except that PTP1B [1 part GST−PTP1B to 10 parts DADE(F_2Pmp)L] was included in the sample. The emergence of the cross-correlation signals is ascribed to the adoption of a specific conformation imposed on the peptide during its residence time on PTP1B. If an interaction "on rate" is assumed to be diffusion-controlled (ca. 10^7 M^{-1} s^{-1}), then from an apparent dissociation constant of about 10^{-6} M, as estimated from the IC_{50} of the peptide, the peptide "off rate" would be on the order of 10−100 s^{-1}. This estimate is consistent with the observation of the transferred nOe cross-peaks.

In an attempt to rule out the possibility of nonspecific binding or the influences of changing the solution viscosity by adding the PTPase, several control studies were carried out. In one set of experiments, GST, instead of GST−PTP1B, was included during sample preparation. In a second set of experiments, alkaline phosphatase replaced GST−PTP1B in the samples, while bovine serine albumin (BSA) was utilized in the third set of experiments. Both alkaline phosphatase and BSA are similar in molecular weight to GST−PTP1B and will influence the solution viscosity to a similar extent. No significant changes in the NOESY spectra from those of DADE(F_2Pmp)L in the protein-free solutions were observed. The results of these experiments, together with the fact that DADE(F_2Pmp)L is an excellent inhibitor of PTP1B, strongly support the conclusion that the nOe cross-peaks have their origin in active-site binding of the oligopeptide. In a final set of experiments, excess vanadate was included in the GST−PTP1B/DADE(F_2Pmp)L medium. In this case, the transfer nOe signals were strongly attenuated, a result in keeping with a competition between two inhibitors for the active site.

With observation of the NOESY signals, it was possible to sequence the peptide and assign the Asp988 and Asp990 signals. The signal assignments are provided in Table 1. The cross-peaks in the transferred NOESY spectrum corresponded to either intraresidue ($NH_i/CH_{\alpha i}$ and $NH_i/CH_{\beta i}$) or sequential ($NH_i/CH_{\alpha i}$ and $NH_{i+1}/CH_{\beta i}$) transferred nOes. No

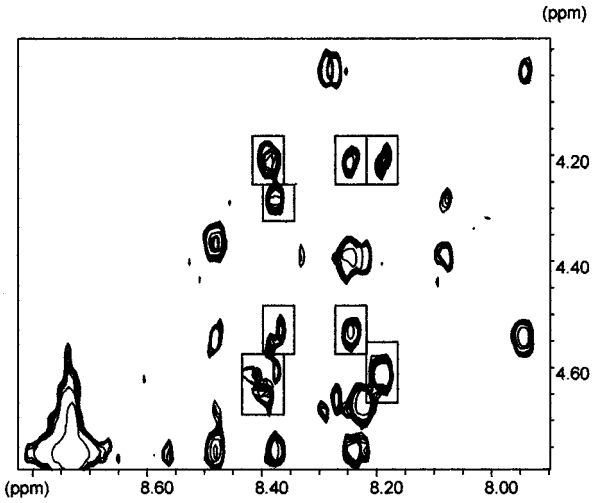

FIGURE 3: NH−CHα fingerprint region of the transferred nOe spectrum of DADE(F_2Pmp)L and IRK1154 in the presence of GST−PTP1B. Cross-peaks originating from DADE(F_2Pmp)L are designated by the rectangles. Conditions of the experiments: DADE(F_2Pmp)L 2 mM; IRK1154 2 mM; pH 7.0; temperature 298 K; mixing time 150 ms.

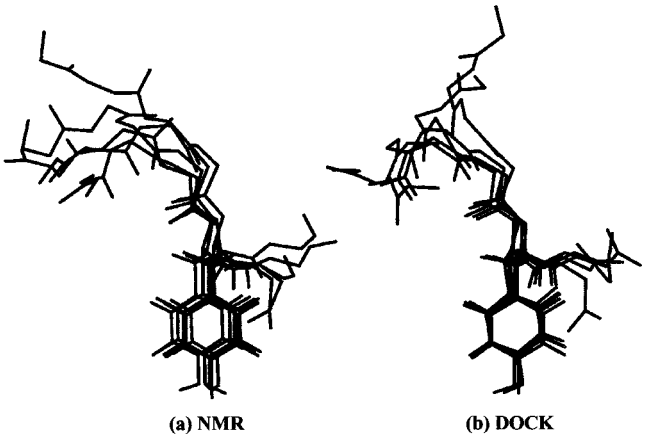

FIGURE 4: Ensembles of distance geometry structures calculated for PTP1B-bound DADE(F_2Pmp)L. Five representative structures chosen at random from the complete set of 500 conformers are shown. For clarity, only the backbone atoms of residues Asp988−Leu993 together with the side chain of DADE(F_2Pmp)L are depicted. The five highest ranked conformers from the complete ensemble, ranked according to a docking protocol (see text), are compared against the active site of PTP1B.

extended pattern of nOe cross-peaks was observed between NH_{i+1}/NH_i pairs as would be expected if the peptide adopted a helix-like structure. The nOe connectivities were consistent with an extended conformation except that weak NH_{i+1}/NH_i cross-peaks between the Asp990 and Glu991 and also between F_2Pmp992 and Leu993 suggested the presence of a turn or twist away from the fully extended structure. The major remaining aspect of the spectrum was the lack of nOe connectivities within the two N-terminal residues. This suggested that these residues might have significant internal mobility, even while the peptide is bound.

Competitive Binding Experiments. While the transferred nOe cross-peaks observed for the GST−PTP1B/DADE(F_2Pmp)L complex were clearly identifiable (Figure 2b), the overall intensity of these cross-peaks was quite weak. This is because DADE(F_2Pmp)L is a very good inhibitor of PTP1B and has an intrinsically low off rate from the enzyme. As a consequence, magnetization transfer to free peptide is inefficient. Interestingly, it was found that titration of a comparable concentration of a second, lower affinity peptide [e.g., the insulin receptor kinase domain-derived peptide IRK1154, TRDI(sY)ETD] into a DADE(F_2Pmp)L−PTP1B solution significantly *increased* the intensity of the observed DADE(F_2Pmp)L cross-peaks. The resulting spectra (Figure 3) show strong nOe cross-peaks from both bound IRK1154 and DADE(F_2Pmp)L, even though there is over 3 orders of magnitude difference in their inhibition constants (*58*). The addition of an excess of vanadate to this solution virtually eliminated the majority of the observed 2D transferred nOe cross-peaks. This indicated that both of the peptides were competing for, and were bound to, PTP1B. This kind of binding competition has been explained in terms of multiple attachment sites on the target enzyme (*59*). In this process, the less potent IRK1154 peptide competes for accessible but occupied attachment points on GST−PTP1B. This leads to molecular rearrangement as a transient ternary complex between DADE(F_2Pmp)L, IRK1154, and the PTPase is created. The result is an enhanced dissociation of DADE-(F_2Pmp)L. Essentially, the less potent peptide pries the more potent peptide out of the binding-site pocket (*59*). This had the effect of lowering the residence time for DADE(F_2Pmp)L on the enzyme and resulted in an increase in cross-peak intensities for DADE(F_2Pmp)L. The spectra obtained in several competitive binding experiments aided in the accurate analysis of the DADE(F_2Pmp)L spectra and subsequently assisted in the derivation of bound DADE(F_2Pmp)L conformations. Other than an improved signal intensity in the cross-peaks, no differential changes in the signal intensities of the more tightly bound inhibitor were observed. This would be in accord with the formation of a transient ternary complex that would not contribute significantly to the nOe spectrum. Further development of this interesting phenomenon may lead to a very useful protocol for the determination of the bound structures of even more tightly bound enzyme inhibitors.

Bound State Conformations and Rational Conformational Sampling. The observed nOe correlations provided a total of 37 distance restraints for use in determination of the structure of the peptide. The restraints were sorted into distance ranges with appropriate pseudoatom corrections. These distance restraints were used to generate a total of 500 structures. All of these conformers exhibited distance restraint violations less than 0.5 Å and all had stereochemically favorable ϕ, ψ angles. All of the structures calculated fell into a conformational family characterized by a region of well-defined highly homologous structure for the residues proximal to F_2Pmp992 (Asp990, Glu991, and Leu993) and a less well-defined N-terminal region for which a significant amount of rotational freedom was indicated (Figure 4a).

There is a precedent for this type of finding in the literature. For example, in a transferred nOe study of the Shc-bound conformation of the oligopeptide DGL(pY)-QGLS, it was determined that a preferred peptide conformation existed for residues immediately following the pY moiety, while the amino and carboxy termini were disordered (*61*).

Unfortunately, observation of specific intermolecular peptide-enzyme nOes is precluded for proteins that are the size of the GST−PTP1B/DADE(F_2Pmp)L complex of this study. This arises because of the extreme broadening of the protein

resonances. Consequently it is not possible to use such contacts to specify the location of the bound peptide. Nevertheless, the control studies strongly suggested that binding derives only from active-site interactions and consequently the physical geometry of the active site of the enzyme (known from X-ray crystallography) provided an attractive framework for refinement of the set of NMR-derived structures.

Each of the 500 NMR-derived conformers was computationally docked into the active site of PTP1B by using the program DOCK (*47*). This facilitated ranking of the set of conformers according to favorability against an energy grid describing the physiochemical characteristics of the active site. The five conformers that had the lowest energy scores as selected by the docking protocol are depicted in Figure 4b. These conformers, all of which satisfy the NMR constraints, clearly are very similar from residues Asp990 to Leu993. For these residues, the structure of the bound DADE(F_2Pmp)L is reminiscent of a twisted β-strand conformation, with a twist occurring at Asp990 when the peptide binds to PTP1B. The sequential NH_{i+1}/NH_i transferred nOe cross-peaks observed between Asp990 and Glu991 and also between the F_2Pmp992 and Leu993 help to define a twist at the F_2Pmp992 site (*36*). The conformations at the two N-terminal residues were not well-defined in these transferred nOe experiments. This is consistent with a high residual mobility for these amino acids and this would follow from the lack of a significant restriction in the conformation of these residues. Apparently these residues provide only weak contributions to the overall binding interactions.

Comparison with DADE(pY)L. The crystal structure of DADE(pY)L, the phosphotyrosine analogue of DADE(F_2-Pmp)L, has been determined from a complex with the Cys215/Ser mutant of PTP1B (*18*). The most energetically favorable transferred nOe-derived conformer of DADE(F_2-Pmp)L, as determined through the docking protocol, was superimposed on the crystallographic structure of DADE-(pY)L and the structures were compared as shown in Figure 5. The general fold of DADE(F_2Pmp)L, as defined by the NMR data, clearly is very similar to that of DADE(pY)L found in the crystal structure. Similarly, the side-chain orientations of residues Asp990 and Glu991 of DADE(F_2-Pmp)L are comparable to those of the X-ray structure. The region of major discrepancy between structures lies at the N-terminal residues. As noted previously, the positions of these residues are not well-defined by the NMR data, but it is also interesting to note that these positions are also not well defined by the X-ray data. The thermal parameters of the X-ray data rise from about 12 A^2 for the active-site residues to about 55 A^2 for those of the terminal ones. This suggests that, even in the crystal, there is substantial movement of these residues. Interestingly, when the DADE-(pY)L, with a conformation conforming to the X-ray coordinates, was docked into PTP1B it ranked about fifth. The replacement of the serine of the crystal structure by the cysteine of the native enzyme can account for this position on the ranking scale. The ranking itself must be treated with caution since active-site residues are not locked into position and with small structural changes within the active site a different ranking sequence of the 500 structures would be obtained. This is evident from the molecular modeling studies discussed below. Overall, the NMR-derived structure is in excellent agreement with the X-ray structure and this is the critical result.

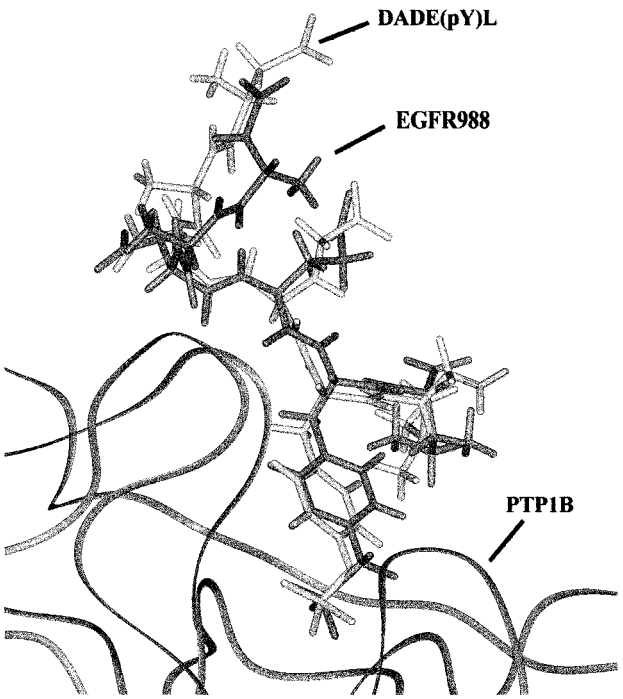

FIGURE 5: Comparison of the crystal structure of DADE(pY)L and the best conformation of DADE(F_2Pmp)L derived from transferred nOe NMR studies. DADE(pY)L is depicted in light gray, DADE-(F_2Pmp)L in dark gray. The backbone of PTP1B is shown in ribbon form. The larger F_2Pmp group of DADE(F_2Pmp)L causes a small offset in the location in the phenyl ring of the docked F_2Pmp compared to the pTyr phenyl ring. The major discrepancy between structures arises at the highly mobile N-terminal residues.

Molecular Modeling Studies. The time evolution of the total energy and temperature of the molecular dynamics simulations of the DADE (F_2Pmp)L−PTP1B complex were investigated for both initialization and production trajectories. The time evolution for total energy and temperature during the initialization phase stabilized after about the first 20 ps of the 34 ps initialization period; this indicating that the system had come to equilibrium. Similarly, during the production trajectory, the lack of significant fluctuations in total energy indicated that the system was stable.

Evolution of the Total Energy and Temperature over 100 ps of Production Molecular Dynamics. To evaluate the efficacy of the 100 ps MD trajectory, an additional 200 ps simulation was performed for the best-ranked DADE(F_2-Pmp)L docked conformation. The dynamic behavior of the peptide throughout the 200 ps of simulation differed little from the 100 ps simulation. Also, in the two cases, similar RMSDs were observed for both peptide and protein residues. Moreover, a similar mode of binding persisted over 200 ps of simulation time. This indicates that, for these systems, 100 ps of production MD is a suitable time period in which to sample the conformational space available to the peptide in its bound conformation. To keep the calculations tractable, the more expeditious time period was utilized in all further simulations.

Molecular dynamics snapshots of the conformation of the DADE(F_2Pmp)L−PTP1B complex as a function of time are depicted in Figure 6. It is evident from the this figure that there are segments of the peptide that undergo only minimal

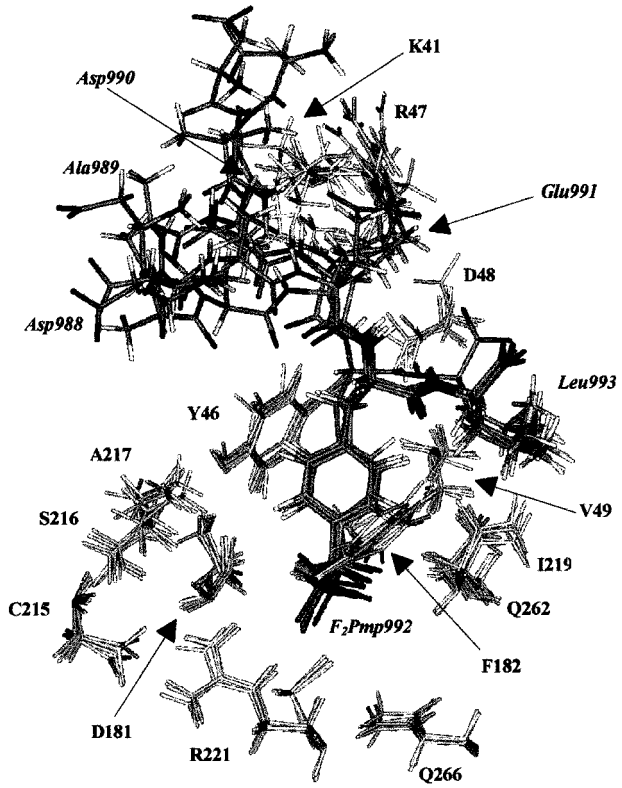

FIGURE 6: Molecular dynamics trajectory for the DADE(F_2Pmp)L−PTP1B complex. Snapshots of DADE(F_2Pmp)L and PTP1B active-site residue conformers extracted from the molecular dynamics trajectory at time intervals of 0, 25, 50, 75, and 100 ps are shown. DADE(F_2Pmp)L residues are depicted in dark gray stick form; PTP1B side chains are represented in light gray stick form.

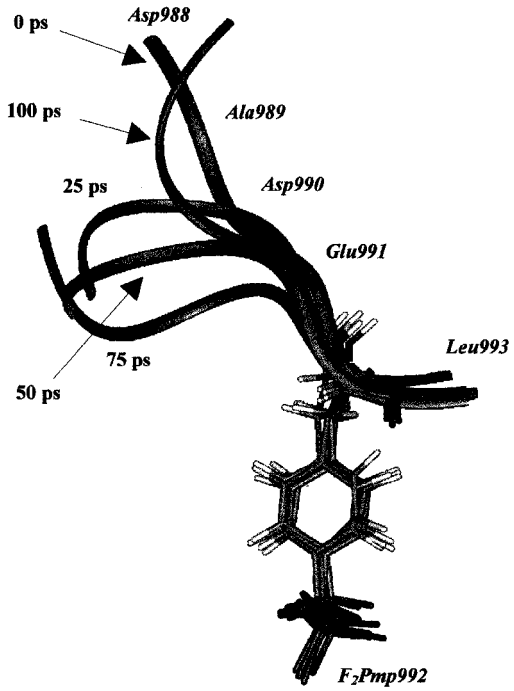

FIGURE 7: Snapshots of DADE(F_2Pmp)L backbone conformations during molecular dynamics simulations. DADE(F_2Pmp)L backbone conformations extracted from the molecular dynamics trajectory at 0, 25, 50, 75, and 100 ps are shown. The backbone is represented in ribbon form and the F_2Pmp moiety is included for clarity.

amounts of motion while other amino acid residues exhibit significant time-dependent fluctuation. As such, the MD snapshots convey critical information regarding which amino acid residues of the peptide experience more or less restriction upon binding to PTP1B. The motion in the peptide backbone during MD simulations is perhaps clarified by concentrating on the fluctuation in the conformation of the backbone atoms as depicted in Figure 7. As demonstrated in Figures 6 and 7, the F_2Pmp and the adjacent residues are motionally restricted during the MD trajectory. However, Asp988 and Ala989 undergo significant changes in their positions during the time course of the simulations. The range of motion indicated for these two residues is consistent with a lack of specific interactions with the enzyme and agrees both with the transferred nOe data and with the high thermal factors observed for the analogous residues in the crystal structure of DADE(pY)L.

DADE(F_2Pmp)L−PTP1B Residue−Residue Interactions. The ability of an inhibitor to complex with an enzyme (as represented by the inhibitor's IC_{50} or K_i) is the consequence of a number of complex molecular interactions. Specifically, binding affinity for the formation of an inhibitor−protein complex involves changes in various intramolecular, intermolecular, and solvation energies associated with reactants (inhibitor, protein) and product (inhibitor bound to protein). Although electrostatic and hydrogen-bonding interactions significantly contribute to the binding affinity between a protein and bound ligand, their effects are often greatly moderated by solvation. Indeed, desolvation of a polar moiety on a ligand and its complementary group on a protein may cost as much in terms of enthalpy as is gained by bringing the two groups together. The net balance typically represents a small difference between large numbers. With this caveat in mind, it is still beneficial to understand the nature of protein−inhibitor interactions and to determine how these interactions contribute to the total binding energy of the inhibitor in the active site of the enzyme.

Interaction energies between DADE(F_2Pmp)L and PTP1B were measured on a residue-by-residue basis following energy minimization of the protein−peptide complex as described in the Materials and Methods section. Each interaction term consists of a combination of electrostatic and van der Waals energies arising from interactions of DADE(F_2Pmp)L with surrounding protein residues. Residues Asp990, Glu991, F_2Pmp992, and Leu993 of DADE(F_2Pmp)L make significant interactions with PTP1B, in terms of both scope and magnitude. In contrast to the multiple peptide−protein interactions observed at the binding pocket, the interactions at P(−4) and P(−3) were much weaker, indicating little contact with the enzyme for the N-terminal and adjacent residues. The total interaction energy for each residue of DADE(F_2Pmp)L are indicated in Table 2. Interestingly, it appears that Asp990 and Leu993 had the strongest interaction with the protein, followed by Glu991. The interactions for Asp990 and Glu991 are almost fully electrostatic in nature and may possibly be diminished by the influences of solvation. In contrast, the interaction between F_2Pmp992 and PTP1B was primarily achieved through van der Waals contacts.

The pattern of data suggests that the binding of peptide-based substrates or inhibitors to PTP1B is a cooperative event involving the recognition of the pTyr functional group, or mimic, as well as interactions with structural features from residues flanking it. The total interaction energy between

Table 2: PTP1B−DADE(F_2Pmp)L Interaction Energies: Comparison to DADE(pY)L[a]

DADE(F_2Pmp)L	Asp988	Ala989	Asp990	Glu991	F_2Pmp992	Leu993	all
vdW[b]	−0.37	−0.64	−4.99	−3.84	−35.67	−9.69	−55.20
elect.[c]	−1.64	−2.55	−169.80	−134.97	−23.79	−119.35	−452.10
TIE[d]	−2.01	−3.19	−174.80	−138.81	−59.46	−129.04	−507.30
DADE(pY)L[e]	Asp988	Ala989	Asp990	Glu991	(pY)992	Leu993	all
vdW[b]	−1.12	−1.37	13.63	−8.65	−1.54	−3.80	−2.85
elect.[c]	66.03	1.97	−201.82	−135.98	−8.83	6.99	−271.64
TIE[c]	64.91	0.60	−188.19	−144.63	−10.37	3.19	−274.49

[a] Energies are given in kilocalories per mole. [b] van der Waals interaction energy. [c] Electrostatic interaction energy. [d] Total interaction energy. [e] Interaction energy was calculated for DADE(pY)L in its crystal orientation (*18*). Calculations were performed in a solvent sphere (15 Å inner shell, 5 Å outer layer).

Table 3: Contribution to the Total Interaction Energy between DADE(F_2Pmp)L and PTP1B from Various Component Energies

interaction	energy (kcal/mol)
total interaction energy with both solvent and enzyme	−605.3
total interaction energy with solvent	−98.0
total interaction energy with enzyme	−507.3
total van der Waals interaction energy with enzyme	−55.2
total electrostatic interaction energy with enzyme	−452.1

DADE(F_2Pmp)L and PTP1B may be partitioned into the component energy terms. As can be seen from Table 3, van der Waals energy contributed about 11% of the total interaction energy (−55.2 kcal/mol), while electrostatic terms accounted for the remaining 89% (−452.1 kcal/mol). Even allowing for the effects of desolvation, this strongly suggests that the DADE(F_2Pmp)L−PTP1B binding interaction is predominantly electrostatic in nature.

Orientation of the Bound Peptide. The overall topology of the active site of PTP1B is relatively uneven and is marked with several clefts and protuberances. The phosphotyrosine binding pocket is located approximately midway across a relatively flattened groove on the surface of the enzyme, flanked on one side by a wall of basic amino acids. According to the model proposed in this work, DADE(F_2-Pmp)L is bound to PTP1B in a twisted β-strand conformation along a narrow trough located on the surface of the enzyme. The peptide is anchored to the enzyme by interactions to the active-site pocket itself, as well as by contacts to PTP1B amino acids that protrude from the molecular surface adjacent to the binding cleft. With the F_2Pmp of DADE(F_2Pmp)L buried in the PTP1B binding pocket, residues Asp990−Leu993 lie within the binding groove itself, while the N-terminal residues, Asp988 and Ala989, project out of the active site (Figure 8). The binding of DADE(F_2Pmp)L to PTP1B buries approximately 520 Å^2 of the surface area accessible to solvent in the free peptide and 382 Å^2 of the surface area accessible to solvent in unliganded PTP1B.

DADE(F_2Pmp)L Backbone Interactions with PTP1B. Analysis of the model of the bound DADE(F_2Pmp)L suggested that it forms a number of strong, stable hydrogen bonds with various residues flanking the active-site pocket of PTP1B. In particular, in the model the backbone amido protons of F_2Pmp992 and Leu993 form strong hydrogen bonds with the carboxyl side chain of PTP1B residue D48 (Figure 9). In addition, a hydrogen bond is also formed between the amide proton of R47 and both the backbone and side-chain carbonyls of the DADE(F_2Pmp)L residue,

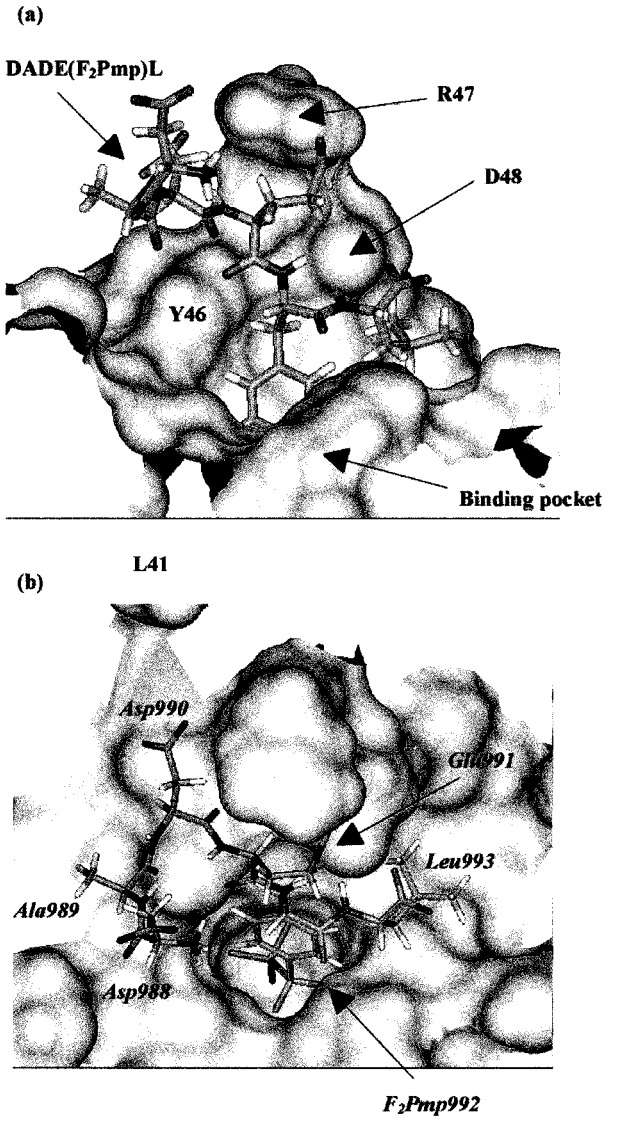

FIGURE 8: Representation of DADE(F_2Pmp)L bound in the active site of PTP1B. DADE(F_2Pmp)L is depicted in stick form. The surface of PTP1B is represented in shades of gray and represented as a solvent-accessible (Connolly) surface (probe radius 1.4 Å) (*40*, *41*).

Asp990 (Table 4). These bonds may determine the peptide conformation at the F_2Pmp position and help explain why the peptide adopts a twisted β-strand in this region, as reflected in the transferred nOe data. Additional but weaker water-mediated hydrogen bonds formed intermittently during the MD simulations but did not persist throughout.

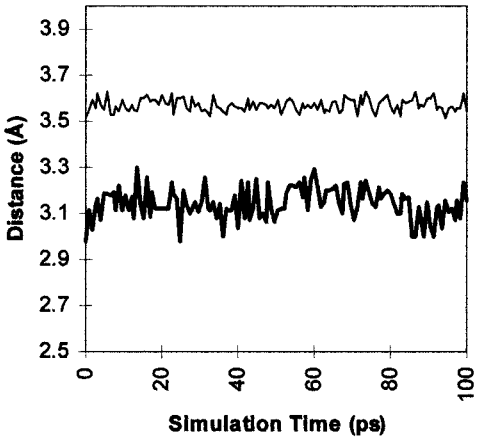

FIGURE 9: Distance between the F_2Pmp992 and Leu993 backbone amide protons and the D48 side chain as a function of simulation time The carboxyl side chain of D48 is defined as a pseudoatom, X (X = midpoint of Cγ, Oδ_1, and Oδ_2). Thin line (~3.6 Å), F_2-Pmp992 NH−D48 X; thick line (~3.1 Å), Leu993 NH−D48 X. The stability of the interactions over the entire course of the simulation is evident from the plot. Distances are given in angstroms.

DADE(F_2Pmp)L Side-Chain Interactions with PTP1B: (A) Asp988 and Ala989: Neither the backbone nor the acidic side chain of Asp988 made significant contacts with the enzyme during the MD simulations. This suggests that residues situated at positions P(−4) (P refers to the phosphotyrosine position) play only a minor role in substrate/inhibitor binding to PTP1B (Table 2). Model building studies suggested that acidic residues at P(−3) might make long-range interactions with basic residues located in the vicinity of the active-site pocket (e.g., K36, K41). With Ala989 at P(−3) no significant peptide−protein interactions were noted in the model (Table 2). These findings are in accord with experimentation; Asp988 and Ala989 exhibited only very limited, weak transferred nOe cross-peaks, consistent with inhibition data presented in the literature (*62*−*63*).

(B) Asp990 and Glu991. Kinetics studies have indicated that peptides with acidic side chains N-terminal to pTyr are good substrates for many PTPases, including PTP1B (*64*, *65*). In the model described here, electrostatic interactions between acidic residues on DADE(F_2Pmp)L and basic PTP1B residues confer considerable binding affinity for the peptide (Table 2). The side chain of Glu991 forms a strong ion pair with the guanidino side chain of the PTP1B, R47. The carboxylate oxygens of Glu991, OE1 and OE2, are roughly equidistant from the guanidino NH_1 and NH_2 nitrogens of R47 and are at near-optimum distance for such a contact (Table 4) (*66*). The interaction energy for the formation of this ion pair is very high (−81 kcal/mol), underscoring its potential contribution to the overall free energy of binding. Similarly, the donor−acceptor distance is retained with little fluctuation throughout the course of the simulation.

In the crystallographically determined structure of DADE-(pY)L, the carboxylic side chain of Asp[P(−2)] is purported to form an ion pair (~3.7 Å) with the $NH_1(\eta_1)$ proton of R47. However, in these MD simulations the side chain of Asp990 rotated away from R47 during the course of the trajectory and stretched across the surface of the enzyme so as to make contact (~4 Å) with K41. This occurrence suggests that substitution for the longer and more flexible glutamate residue at the P(−2) position would confer additional binding affinity. Inspection of the total interaction energy for Asp990 in the model suggests a key electrostatic binding role for this residue (Table 2).

(C) F_2Pmp992. The calculated interaction energy between the F_2Pmp group and PTP1B consisted of both van der Waals (−35.7 kcal/mol) and electrostatic (−23.8 kcal/mol) terms (Table 2). The van der Waals interactions arise mainly through nonpolar interactions with residues lining the walls of the PTP1B binding pocket, as well as through contributions from aromatic stacking interactions. The electrostatic interactions had their main source in a complex network number of hydrogen bonds to the pTyr phosphate analogue. The main-chain amide protons of residues S216−R221 of PTP1B make a number of close contacts with the three terminal phosphonate oxygens of F_2Pmp (Table 4). This suggests that a network of hydrogen bonds is generated within the active site. These hydrogen bonds are similar to those observed to the phosphate group in the X-ray structure of DADE(pY)L (*18*). Additionally, the guanidinium side chain of R221 makes electrostatic contacts to the O2, O4, and O5 atoms of the phosphonate moiety of F_2Pmp, while D181 makes a water-mediated hydrogen bond to O2. In the model, these are generally strong, stable hydrogen bonds that are retained with little fluctuation throughout the MD trajectory (<0.5 Å deviation). An additional source of binding affinity suggested by the model is realized through the fluorine atoms of F_2Pmp. In a recently determined crystal structure, it was noted that the *pro-R* fluorine atom of [1,2-difluoro-1-(2-naphthalenyl)methyl]phosphonic acid makes an unconventional F−HN hydrogen bond (~2.4 Å) to the amido group of F182 (*67*). The formation of a similar bond was observed in this model (F_1−HN ~2.02 Å).

The large number of hydrogen bonds formed upon binding of DADE(F_2Pmp)L will offset much, if not all, of the energetic penalty associated with desolvation of the charged phosphonate group. Also, hydrophobic displacement of bound water molecules is likely to significantly contribute to the binding affinity of the peptide. The classical hydrophobic effect is caused by the release of water molecules with a corresponding gain in entropy (*68*).

Burying the hydrophobic surface area of a ligand in the hydrophobic sites on a protein provides an important driving force for protein−ligand complexation. As both ligand and protein hydrophobic surfaces come into contact, water molecules are released in an energetically favorable process. It has been estimated that phosphotyrosine represents 53% of the solvent-accessible surface area of DADE(pY)L (*18*). Similarly, the side chain of the F_2Pmp accounts for essentially 30% of the total accessible surface area of DADE(F_2Pmp)L (280 Å^2). According to the model, when bound to PTP1B, approximately 90% of the F_2Pmp side chain is buried within the PTP1B binding pocket. Assuming that each single buried square angstrom contributes ~−0.025 kcal/mol (*69*), a possible contribution of about −6 kcal/mol to the overall free energy of binding may be estimated on the basis of hydrophobic considerations when F_2Pmp is buried in the active-site pocket.

Several nonpolar residues flank the active-site pocket of PTP1B and make favorable contacts to the phenyl ring of F_2Pmp in the modeled complex. In particular, the side chains

Table 4: Potential Hydrogen Bonds Identified in the Modeled Interaction between DADE(F_2Pmp) and PTP1B[a]

donor atom (D)	hydrogen atom (H)	acceptor atom (A)	distance H−A (Å)	angle D−H−A (deg)
R24 NH2	R24 HH21	Leu993 O_{term}	3.48	111.14
R47 N	R47 HN	Asp990 CO	3.88	165.12
R47 N	R47 HN	Asp990 OD1	3.87	116.90
R47 N	R47 HN	Asp990 OD2	3.99	107.33
R47 NE	R47 HE	Glu991 OE1	3.89	130.12
R47 NH1	R47 HH11	Glu991 OE1	3.64	136.35
R47 NH1	R47 HH11	Glu991 OE2	1.78	152.85
R47 NH2	R47 HH21	Glu991 OE1	1.85	140.17
R47 NH2	R47 HH21	Glu991 OE2	3.33	96.03
R47 NH2	R47 HH22	Glu991 OE2	3.23	102.41
F182 N	F182 HN	F2Pmp992 O2	3.76	156.75
S216 N	S216 HN	F2Pmp992 O2	3.47	159.59
S216 N	S216 HN	F2Pmp992 O5	3.00	118.76
A217 N	A217 HN	F2Pmp992 O4	3.31	128.68
A217 N	A217 HN	F2Pmp992 O5	2.09	176.38
G218 N	G218 HN	F2Pmp992 O4	3.88	103.56
I219 N	I219 HN	F2Pmp992 O4	2.85	136.40
G220 N	G220 HN	F2Pmp992 O2	3.67	114.67
G220 N	G220 HN	F2Pmp992 O4	1.89	152.93
R221 N	R221 HN	F2Pmp992 O2	2.74	164.27
R221 N	R221 HN	F2Pmp992 O4	3.69	129.95
R221 NE	R221 HE	F2Pmp992 O2	1.98	173.22
R221 NE	R221 HE	F2Pmp992 O5	3.95	150.95
R221 NH2	R221 HH22	F2Pmp992 O2	2.93	130.00
R221 NH2	R221 HH22	F2Pmp992 O5	3.39	143.62
Q262 NE2	Q262 HE22	Leu993 O'T	1.78	168.52
Q262 NE2	Q262 HE22	Leu993 CO	3.82	161.41
F2Pmp992 N	F2Pmp992 HN	D48 OD1	2.05	150.77
F2Pmp992 N	F2Pmp992 HN	D48 OD2	3.18	113.85
Leu993 N	L993 HN	D48 OD1	2.74	132.24
Leu993 N	L993 HN	D48 OD2	1.90	169.27

[a] Hydrogen bonds were determined following energy minimization to convergence. A 4.0 Å cutoff is used. Hydrogen bonds were defined according to a relaxed acceptor−donor distance and D−H−A geometry protocol (*97*), consistent with the resolution of the PTP1B X-ray crystal structure (2.8 Å) (*18*).

of Y46, V49, F182, A217, and I219 and the aliphatic moieties of Q262 and Q266 provide an amphipathic environment conducive to binding and make several nonspecific van der Waals contacts with F_2Pmp992 (∼3−4 Å). The side chains of Q262 and Q266 were noted to displace slightly during MD (<0.25 Å) so as to make more favorable contacts with the peptide. The mobility of Q262 within the active-site pocket has been confirmed by crystallographic data (*70*).

The most significant PTP1B side-chain perturbation noted during the MD simulations was for K120, which shifted by ∼1.50 Å during the trajectory. In the original docked orientation, the K120 NH_3^+ basic headgroup was poorly oriented with respect to the phenyl ring of F_2Pmp. However, during 250 ps of MD simulations, it rotated to present a more favorable exposure to the aromatic ring of F_2Pmp. The importance of such cation−π interactions in biological systems has received attention in the literature (*71*, *72*). Electrostatic interactions between cationic arginine or lysine and aromatic rings of phenylalanine, tyrosine, or tryptophan can be quite strong, contributing as much as ∼10−20 kcal/mol in the gas phase (*72*). The less than ideal parallel stacked orientation of K120 relative to F_2Pmp at the start of the MD simulation explains the poor interaction energy noted between these residues (+2.55 kcal/mol). The original orientation of K120 was that observed in the crystal structure of PTP1B and might arise because of crystal packing forces. Rotation of K120 within the active site resulted in a favorable interaction energy when K120 was oriented perpendicular to the phenyl ring of F_2Pmp (Figure 10). In concert with this rotation, other compensatory rearrangements occur within the active site.

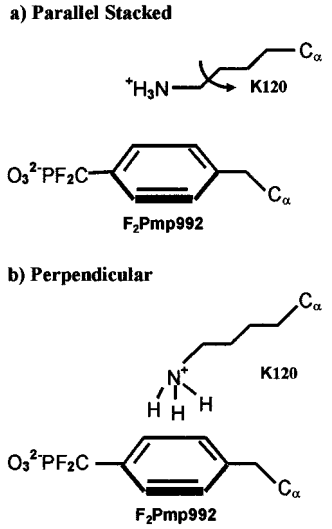

FIGURE 10: Representation of the cation−π stacking interaction between K120 and F_2Pmp. Side-chain representations of the amino−aromatic interaction between K120 and F_2Pmp992 are shown. In the initial docked structure (a), the NH_3^+ headgroup of K120 is oriented in an unfavorable stacked geometry relative to the phenyl ring of the F_2Pmp (Nζ−π ∼4.3 Å). During molecular dynamics simulations (b), the K120 side chain rotates so as to present a more favorable perpendicular face to the phenyl ring.

An important source of peptide−protein binding interactions is mediated through interactions between the phenyl

ring of F_2Pmp and the aromatic rings of Y46 and F182 (−4.1 and −4.9 kcal/mol respectively; Table 2). Specific interactions between aromatic rings give rise to important forces in molecular recognition because they play a key role in controlling the conformations and substrate-binding properties of nucleic acids and proteins (*73*, *74*).

Aromatic or $\pi-\pi$ stacking complexes are subject to stabilization from both dispersive and electrostatic sources (*75*). Only edge-to-face (tilted T) and parallel and offset stacked interactions are energetically favorable. Both tilted T and offset interactions have been observed in proteins. Apparently, neither is preferred over the other (*73*, *74*, *76*). The optimal centroid−centroid distance between stacked aromatic rings has been reported to be in the range 4.5−7.0 Å (*75*−*77*). The aromatic stacking observed between the phenyl ring of F_2Pmp and F182 in the modeled complex corresponds to a favorable tilted T arrangement (centroid−centroid distance = 5.7 Å), following a χ_1 rotation of ∼18° during the MD (<0.3 Å RMSD). Similarly in the model, Y46 stacks in an analogous manner (centroid−centroid distance = 5.3 Å) relative to the phenyl ring of F_2Pmp and rotates ∼12° during the course of the MD trajectory in order to present a more complementary interaction plane (<0.2 Å RMSD). The phenyl ring of F_2Pmp itself was very stable over the entire simulation. Aromatic stacking interactions may contribute as much as 2.0 kcal/mol to the total free energy of binding for each residue involved in the interaction (*77*). This underscores the potential significance of these interactions in terms of the recognition of substrates by the PTPases.

Detailed studies have confirmed that the (difluorophosphonomethyl)phenylalanine functionality confers significant binding affinity (1000 times more potent) compared to unsubstituted phosphonate (*62*). Manual rotation of the F_2Pmp functionality revealed a marked correlation between the orientation of the F_2Pmp moiety and the interaction energy. To help understand the potency of F_2Pmp-containing peptides, additional 100 ps MD trajectories were recorded for DADE(F_2Pmp)L, but with the F_2Pmp moiety rotated in a number of different orientations within the active-site pocket. These simulations showed that the lowest energy conformation of F_2Pmp occurred when the Cη carbon atom occupied the approximate position of the phenolic oxygen of phosphotyrosine in the DADE(pY)L X-ray crystal structure (*18*). Moreover, the active-site residues themselves were most stable, in a dynamic sense, when F_2Pmp was oriented in this manner. The alternative orientations resulted in significant perturbations within the active site, with Y46, D181, F182, and Q262 moving substantially during the simulations.

It is likely that key aromatic stacking configurations are lost when the phenyl ring of F_2Pmp deviates from the optimum position determined in the modeling simulations. Indeed, in modeling studies, deviations were found to compel the phenyl rings of Y46 and F182 to reorient within the binding site to prevent energetically unfavorable interactions (e.g., face-to-face stacking). However, aromatic stacking fails to explain the 1000-fold potency of F_2Pmp compared to its Pmp analogue.

Inspection of the modeled complex suggested that a significant factor in determining the potency of F_2Pmp is the formation of a strong, stable hydrogen bond between the *pro*-R fluorine atom of F_2Pmp and the amido nitrogen of F182 (F−HN 2.02 Å). A similar bond was also observed in the bound structure of a difluoronaphthalenyl ligand (*67*). A notable reduction in interaction energy (>30%) was observed when F_2Pmp was modeled with this fluorine removed, supporting the stereospecific significance of this interaction. It is apparent that within the preorganized binding site of the enzyme the *pro-R* fluorine atom is optimally orientated in terms of both contact distance (2.02 Å) and D−H−A angle (∼127°), with respect to the amide proton of F182, to significantly affect binding affinity. Interestingly, these findings are consistent with the recently determined crystal structure of a dinitrophenylhydrazone (*78*), where a short F−H contact (2.02 Å) of similar geometry (D−H−A 125°) was observed. In addition to this primary interaction, the $N\epsilon H_{(2)}$ proton of Q266 makes a water-mediated hydrogen bond via a crystallographically resolved water molecule to the alternative fluorine atom in the bound model (F_2−O−H−O−HN ∼3.2 Å/bond). Modeling suggests that this latter interaction is far weaker than the former. This is consistent with inhibition data that indicates that *pro-R* monofluorinated Pmp is as effective an inhibitor as difluorinated Pmp (*67*). The formation of this F−H hydrogen bond helps to explain why difluorophosphonomethyl-containing peptides are more potent inhibitors than their phosphonomethyl analogues. These findings agree with a recent study that suggests that F−HN contacts, particularly to aliphatic C(sp^3)−F fluorine atoms, are sufficiently stabilizing interactions to significantly influence binding energies (*79*).

(D) Leu993. It has been noted that the flexible hydrophobic side chains of peptides prefer to make nonspecific van der Waals contacts with the surface of a protein rather than be exposed to solvent. This phenomenon has been referred to as hydrophobic collapse (*80*). The nonpolar side chain of the leucine of DADE(F_2Pmp)L is located on a shallow hydrophobic patch on the surface of PTP1B and undergoes hydrophobic collapse during the modeling simulations. Along the surface of the enzyme, it forms various nonspecific van der Waals contacts with the side chains of PTP1B residues Y46, V49, A217, I219, M258, and Q262 (<4 Å).

In addition to the energy arising from these van der Waals contacts, the interaction energy calculated for Leu993 in the bound model also contains a considerable electrostatic component. In particular, the −COOH terminus of the leucine makes a number of charged interactions with PTP1B, such as with R24 and Q262 (Table 2). Indeed, positively charged residues are found to be highly disfavored at this position (*64*, *65*), presumably because of unfavorable electrostatic interactions with basic residues at the P(+*X*) site (e.g., R24 and R254). A shallow pocket is located proximal to the primary binding site on PTP1B (Figure 7). This region is purported to represent a secondary, low-affinity PTPase binding site (*81*). Model building indicates that a glutamate residue at P(+1) may interact with residues in the secondary binding site. This hypothesis is supported by an inhibition study, in which the X substituent of the general sequence DE(sY)X was systematically varied (*13*). Inhibition was greatest when X was large and bulky (increased van der Waals contacts) or was acidic and was the poorest when X was a basic amino acid. This suggests that the P(+*X*) zone of PTP1B can tolerate a variety of substituents.

Molecular Modeling of DADE(pY)L. To provide a useful comparison for the results of these molecular modeling

simulations, the X-ray crystallographic structures corresponding to the DADE(pY)L−PTP1B complex and that of PTP1B alone (*18*) were subjected to the same energy minimization and molecular dynamics protocol as that described here for DADE(F_2Pmp)L. Residue-specific deviations from the crystallographically determined positions of the DADE(pY)L residues following 100 ps of MD were very similar to those noted for DADE(F_2Pmp)L. Specifically, Asp[P(−4)] and Ala[P(−3)] of DADE(pY)L exhibited similar conformational flexibilities to those of Asp988 and Ala989 of DADE(F_2Pmp)L. Similarly, pTyr, and the residues flanking it, were conformationally restrained by the protein. Fluctuations in the positions of PTP1B active-site residues of the DADE(pY)L−PTP1B complex were not much different from those observed for the DADE(F_2Pmp)L−PTP1B system. Slight differences were noted in the orientations observed for D181 and F182 of PTP1B in the presence of DADE(pY)L as opposed to DADE(F_2Pmp)L. This reflects the bulkiness of F_2Pmp compared to phosphotyrosine. Overall, the set of hydrogen-bonding, electrostatic, and van der Waals interactions observed for the DADE(pY)L model were similar to those of DADE(F_2Pmp)L.

A summary of the total interaction energies calculated for DADE(pY)L in its crystal orientation is presented in Table 2. Overall, the binding interactions are generally consistent for both analogues of the EGFR sequence. However, several key differences warrant explanation. First, in its crystallographic orientation, D[P(−4)] makes several unfavorable electrostatic contacts with PTP1B residues in the active site, notably with K41, R45, and R47. Energy minimization significantly diminished these deleterious contacts. Similarly, it is interesting to note that D[P(−2)] of DADE(pY)L was found to reorient relative to K41 during the course of the MD simulation and made a long contact with it, as similarly observed for Asp990 in the DADE(F_2Pmp)L modeling studies. This configuration may therefore represent a favorable situation for the D[P(−2)] side chain and suggests that the orientation observed in the crystal structure may be due to crystal packing forces rather than as a consequence of specific interactions with R47. The X-ray structure may represent a conformation accessible to the complex under native conditions but need not be the most probable solution structure (*82*). This notion is further supported by interaction energy calculations. The calculated interaction energy between D[P(−2)] and R47 in the original crystal orientation reveals that D[P(−2)] makes a very unfavorable van der Waals contact with the side chain of R47 (>+20 kcal/mol). During energy minimization, D[P(−2)] reoriented so as to mitigate this clash. Similarly, more favorable interactions between pTyr and residues lining the active site pocket of PTP1B were realized following molecular modeling, in particular in terms of electrostatic interactions with D181 and van der Waals contacts with Y46 and F182. The potency of the F_2Pmp moiety as compared to phosphotyrosine is underscored by the differences in interaction energies calculated for the two analogues (Table 2). In the crystal structure of DADE(pY)L, the −COOH terminus at P(+1) is pointed away from the surface of the enzyme and therefore does not make contact with PTP1B residues. This is reflected in the poor interaction energy calculated for L[P(+1)] of DADE(pY)L. However, following energy minimization and molecular dynamics of the crystallographically derived complex, L[P(+1)] was able to maximize van der Waals contacts on the surface of the enzyme, while the carboxyl terminus made favorable interactions with R24 and R254. These modeling studies therefore suggest that the orientation of DADE(pY)L observed in the crystal structure is not necessarily the orientation adopted when the peptide−PTP1B complex is in solution.

Molecular Modeling of Unligated PTP1B. Energy minimization and 100 ps of molecular dynamics simulations were performed on unligated PTP1B. The calculations were done on the "closed loop" (WPD loop) conformation. This loop is a PTP1B surface loop that, when closed, brings the catalytic aspartate residue into the active site. These studies corroborated the molecular modeling performed on the liganded complexes. Specifically, these simulations suggest that conformational changes in the enzyme during EM and MD are relatively small and are localized to the immediate vicinity of the pTyr pocket. In the absence of bound ligand, PTP1B residues flanking the active site exhibited more conformational flexibility than when peptide was present. Perhaps this is to be expected physiologically, because in the absence of bound ligand the WPD loop (residues 179−187) could well open for the admission of substrate. With the exception of movement of the WPD loop, only minor conformational differences between the unligated PTP1B and the corresponding ligated crystal structures (*18*, *83*) were observed after the dynamics simulations were completed. Also, in general, molecular modeling performed on PTP1B in the presence and absence of ligand yielded comparable results. There was no suggestions from the modeling studies that the free enzyme was unstable (*84*).

CONCLUSIONS

NMR nOe enhancement studies have been utilized to obtain a structural model for the inhibition of PTP1B by the potent inhibitor DADE(F_2Pmp)L. This inhibitor is based on a 6 amino acid peptide from the epidermal growth factor receptor segment commencing at EGFR988. DADE(F_2Pmp)L binds to a narrow trough on the surface of PTP1B and adopts a twisted β-strand conformation. Relatively small, localized changes in the conformation of PTP1B accompany peptide binding during the MD simulations. Hydrogen bonds between the side chain of D48 and the backbone amide NH protons of F_2Pmp992 and Leu993 stabilize a pseudo-α-helical conformation at the F_2Pmp position. The side chain of F_2Pmp is buried within a deep binding pocket on the surface of the enzyme and is secured in place by a complex network of hydrogen-bonding interactions to backbone amide protons of several PTP1B residues that line the base of the pocket. Ion pairs between the positively charged PTP1B residue R221 and the phosphonate help stabilize this interaction. Nonpolar residues flank the sides of the pocket, creating an amphipathic environment conducive to binding. The phenyl rings of Y46 and F182 of PTP1B stack in an energetically favorable tilted T configuration with the phenyl ring of F_2Pmp. An unusually strong F−HN bond confers additional binding affinity. Sequence specificity is conferred through interactions between acidic groups on DADE(F_2Pmp)L and positive residues in the vicinity of the binding cleft, notably R47. Nonspecific van der Waals interactions between Leu993 and nonpolar PTP1B surface residues complete the pattern of interaction. This model adequately

Chart 1: DADE(F_2Pmp)L−PTP1B Interaction Summary

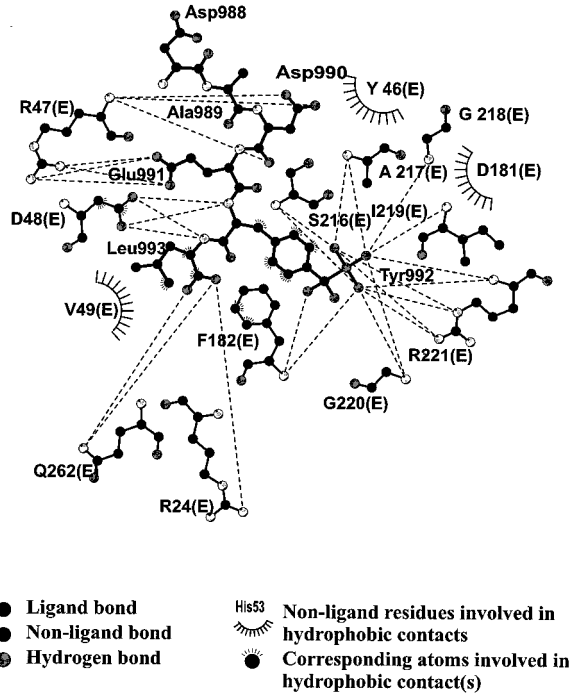

accounts for the experimentally measured potency of the inhibitor (*62*). The major contributions to the binding interactions are summarized in Chart 1.

The extended conformation is the most common recognition motif in peptide−protein complexes (*85*, *86*). Peptide−protein interactions based on an extended peptide conformation have been observed in complexes with HIV-1 protease (*87*, *88*), MHC molecules (*89*, *90*), and phosphotyrosine-containing peptides bound to SH2 domains (*91*, *92*). The traditional view that ligand−protein binding strength results mainly from the formation of a reasonable number of hydrogen bonds, as well as the filling of space within the active site, ignores a number of important energetic processes. Indeed, the successful recognition between a peptide and a target protein depends on both the steric and electronic complementarities of the ligand and the active site. Many factors determine the strength of the overall interaction between a peptide and its target enzyme. These include the formation of favorable van der Waals, hydrogen-bonding, and electrostatic interactions and protein and peptide entropy, as well as the role of the solvent (*93*).

In this work, the contributions of energetic and conformational factors to the association of DADE(F_2Pmp)L with PTP1B were studied by energy minimization and molecular dynamics simulations. On the basis of these studies, the binding of this inhibitor to PTP1B is mediated by the formation of hydrogen bonds between PTP1B and the peptide backbone and by electrostatic and hydrophobic contacts with the peptide side chains. The similarity between the NMR-derived structure of DADE(F_2Pmp)L and the X-ray crystallographic structure of DADE(pY)L indicates that the binding interactions of these two entities are very similar. In the crystal structure, binding of DADE(pY)L was conferred via a network of hydrogen bonds between the phosphotyrosine residue and residues lining the cleft of the PTP1B recognition pocket. Additional affinity was provided through nonpolar interactions with the tyrosine ring of the phosphotyrosine moiety (*18*). Similarly, in the model derived here for the binding of DADE(F_2Pmp)L, interactions between the main-chain atoms of DADE(F_2Pmp)L and PTP1B, as well as specific interactions between acidic residues of the peptide and basic residues on the surface of the enzyme, conferred sequence specificity. In particular, the findings of the transferred nOe studies show that residues Glu991−Leu993, and to a lesser extent Asp990, are motionally restricted upon binding to the enzyme, while residues Asp988 and Ala989 lie outside the peptide binding groove. Structural rearrangements occur in both the ligand and the protein upon complexation. This was evidenced by rearrangements from the X-ray-derived orientations of Y46, R47, and F182 of PTP1B during molecular modeling. This may account for the inherent flexibility of the PTP1B active site that would seem necessary to accommodate the diverse variety of substrates that bind to the enzyme (*64*, *94*). Chart 1 provides a diagrammatic representation of the major sources of stabilizing interactions, as suggested by the modeling studies.

The observed pattern of hydrogen bonding between DADE(F_2Pmp)L and PTP1B is somewhat unusual in that backbone−backbone (e.g., R47−Asp990), backbone−side-chain (e.g., Leu993−D48, R47−Asp990), and side-chain−side-chain (e.g., R47−Glu991) interactions occur (*85*, *86*). Typically, one particular form of interaction dominates; for example, protein side chain to peptide backbone interactions [*e.g.*, MHC class I (*89*)], or side-chain to side-chain interactions [e.g., SH2 domains (*92*)]. There are four well-ordered peptide residues within the active site of PTP1B (Asp990−F_2Pmp992). This is a relatively small number when compared with peptide-binding domains of other proteins, which typically bind 5−10 residues (*85*, *86*). Nevertheless, DADE-(F_2Pmp)L achieves a comparable number of contacts with PTP1B as found for other peptide−protein complexes. It makes a significant number of hydrogen bonds (>20; Table 3) and buries over 45% of its solvent-accessible surface area (520 Å^2). In comparison, SH2 domains typically make 8−12 hydrogen bonds with bound peptides and bury roughly 350−550 Å^2 of their surface area (*86*).

Formation of an F−HN bond between the amide proton of F182 and one of the F_2Pmp fluorine atoms confers a remarkable increase in binding affinity when compared to unsubstituted Pmp (*62*). This is because unsubstituted Pmp lacks hydrogen bond-accepting ability at the Cη position (equivalent to the phenolic oxygen of pTyr) and is therefore unable to mimic the hydrogen-bonding interactions that are associated with phosphate- or fluorophosphonate-containing moieties. In the modeled DADE(F_2Pmp)L complex, the F−HN bond to F182 is of near-optimum length and angle (*78*, *79*), and this underscores the importance of geometry in short-range electrostatic interactions. For example, several authors have noted that the most energetically optimal arrangement of donor and acceptor atoms in hydrogen bonding occurs when the two dipole moments are collinear; deviations of 25° reduce the enthalpy of the interaction by at least 10% (a similar attenuation is realized as the bond length is stretched) (*95*, *96*). Therefore, the strength of the F−HN bond as suggested by the modeling studies reflects a situation in which, quite fortuitously, the F−N bond is able to optimally satisfy its geometric requirements. As such, the potency of DADE(F_2Pmp)L may represent a somewhat serendipitous coincidence.

ACKNOWLEDGMENT

Thanks are gratefully extended to the Merck Frosst Centre for Therapeutic Research for the provision of DADE(F_2Pmp), FLAG-PTP1B, and GST−PTP1B. Thanks are particularly extended to Drs. Mike Gresser and Chidambaram Ramachandran for their support and to Dr. Chris Bayly for discussions concerning the molecular dynamics procedures described in this work.

REFERENCES

1. Fischer, E. H., Charbonneau, H., and Tonks, N. K. (1991) *Science 253*, 401−406.
2. Hunter, T. (1995) *Cell 80*, 225−236.
3. Jia, Z. (1997) *Biochem. Cell Biol. 75*, 17−26.
4. Walton, K. M., and Dixon, J. E. (1993) *Annu. Rev. Biochem. 62*, 101−120.
5. Gresser, M. J., and Tracey, A. S. (1990) in *Vanadium in Biological Systems* (Chasteen, N. D., Ed.) pp 63−79, Kluwer Academic Publishers, Dordrecht, The Netherlands.
6. Stankiewicz, P. J., Tracey, A. S., and Crans, D. C. (1995) *Met. Ions Biol. Syst. 31*, 287−324.
7. Stankiewicz, P. J., and Tracey, A. S. (1995) *Met. Ions Biol. Syst. 31*, 259−285.
8. Orvig, C., Thompson, K. H., Battell, M., and McNeill, J. H. (1995) *Met. Ions Biol. Syst. 31*, 575−594.
9. Posner, B. I., Faure, R., Burgess, J. W., Bevan, A. P., Lachance, D., Zhang-Sun, G., Fantus, I. G., Ng, J. B., Hall, D. A., Soo Lum, B., and Shaver, A. (1994) *J. Biol. Chem. 269*, 4596−4604.
10. Shechter, Y., Meyerovitch, J., Farfel, Z., Sack, J., Bruck, R., Bar-meir, S., Amir, S., Degani, H., and Karlish, S. J. D. (1990) in *Vanadium in Biological Systems* (Chasteen, N. D., Ed.) pp 129−142, Kluwer Academic Publishers, Dordrecht, The Netherlands.
11. Tracey, A. S., and Gresser, M. J. (1986) *Proc. Natl. Acad. Sci. U.S.A. 83*, 609−613.
12. Burke, T. R., Jr., Kole, H. K., and Roller, P. P. (1994) *Biochem. Biophys. Res. Commun. 201*, 129−134.
13. Desmarais, S., Jia, Z., and Ramachandran, C. (1998) *Arch. Biochem. Biophys. 354*, 225−231.
14. Fauman, E. B., and Saper, M. A. (1996) *Trends Biochem. Sci. 21*, 413−417.
15. Zhang, Z.-Y., and Dixon, J. E. (1994) *Adv. Enzymol. Relat. Areas Mol. Biol. 68*, 1−36.
16. Bandyopadhyay, D., Kusari, A., Kenner, K. A., Liu, F., Chernoff, J., Gustafson, T. A., and Kusari, J. (1997) *J. Biol. Chem. 272*, 1639−1645.
17. Kenner, K. A., Anyanwu, E., Olefsky, J. M., and Kusari, J. (1996) *J. Biol. Chem. 271*, 19810−19816.
18. Jia, Z., Barford, D., Flint, A. J., and Tonks, N. K. (1995) *Science 268*, 1754−1758.
19. Huyer, G., Liu, S., Kelly, J., Moffat, J., Payette, P., Kennedy, B., Tsaprailis, G., Gresser, M. J., and Ramachandran, C. (1997) *J. Biol. Chem. 272*, 843−851.
20. Bradford, M. M. (1976) *Anal. Biochem. 72*, 248−254.
21. Mach, H., Middaugh, C. R., and Lewis, R. V. (1992) *Anal. Biochem. 200*, 74−80.
22. Nxumalo, F. (1997) Influence of vanadium complexes on the catalytic activity of the protein tyrosine phosphatases, M.Sc. Thesis, Simon Fraser University, Burnaby, British Columbia, Canada.
23. Campbell, A. P., and Sykes, B. D. (1991) *J. Magn. Reson. 93*, 77−92.
24. Cantor, C. R. and Schimmel, P. R. (1980) *Biophysical Chemistry*, W. H. Freeman and Co., San Francisco, CA.
25. Marion, D., and Wüthrich, K. (1983) *Biochem. Biophys. Res. Commun. 113*, 967−974.
26. Piotto, M., Saudek, V., and Sklenár, V. (1992) *J. Biomol. NMR 2*, 661−665.
27. Jeener, J., Meier, B. H., Bachman, P., and Earnst, R. R. (1979) *J. Chem. Phys. 71*, 4546−4553.
28. Bothner-By, A. A., Stephens, R. L., Lee, J.-M., Warren, C. D., and Jeanloz, R. W. (1984) *J. Am. Chem. Soc. 106*, 811−813.
29. Bax, A., and Davis, D. G. (1985) *J. Magn. Reson. 63*, 207−213.
30. Wider, G., Macura, S., Ernst, R. R., and Wüthrich, K. (1984) *J. Magn. Reson. 56*, 207−234.
31. Braunschweiler, L., and Ernst, R. R. (1983) *J. Magn. Reson. 53*, 521−558.
32. Bax, A., and Davis, D. G. (1985) *J. Magn. Reson. 65*, 355−360.
33. Piatini, U., Sorensen, O. W., and Ernst, R. R. (1982) *J. Am. Chem. Soc. 104*, 6800−6801.
34. Rance, M., Sorensen, O. W., Bodenhausen, G., Wagner, G., Ernst, R. R., and Wüthrich, K. (1983) *Biochem. Biophys. Res. Commun. 117*, 479−485.
35. Biosym/MSI (1995) InsightII Molecular Modeling System (95.0), Biosym/MSI, San Diego, CA.
36. Wüthrich, K. (1986) in *NMR of Proteins and Nucleic Acids*, John Wiley & Sons, New York.
37. Biosym/MSI (1995) Discover (2.9.7./95.0/3.0.0), Biosym/MSI, San Diego, CA.
38. Crippen, G. M., and Havel, T. F. (1988) in *Distance Geometry and Molecular Conformation*, John Wiley & Sons, New York.
39. Moseley, H. N. B., Curto, E. V., and Krishna, N. R. (1995) *J. Magn. Reson. B108*, 243−261.
40. Connolly, M. L. (1983) *Science 221*, 709−713.
41. Connolly, M. L. (1983) *J. Appl. Crystallogr. 16*, 548−558.
42. Meng, E. C., Shoichet, B. K., and Kuntz, I. D. (1992) *J. Comput. Chem. 13*, 505−524.
43. Shoichet, B. K., Bodian, D. L., and Kuntz, I. D. (1992) *J. Comput. Chem. 13*, 380−397.
44. Gschwend, D. A. and Kuntz, I. D. (1996) *J. Comput.-Aided Mol. Des. 10*, 123−132.
45. Biosym/MSI (1995) Discover 2.9.7/95.0/3.0.0 User Guide, Part 1, Biosym/MSI, San Diego, CA.
46. Leach, A. R. (1996) in *Molecular Modelling: Principles and Applications*, Addison-Wesley Longman, Ltd., Harlow, Essex, U.K.
47. Oshiro, C. M., Kuntz, I. D., and Dixon, J. S. (1995) *J. Comput.-Aided Mol. Des. 9*, 113−130.
48. Szklarz, G. D., He, Y. A., and Halpert, J. R. (1995) *Biochemistry 34*, 14312−14322.
49. Dauber-Osguthorpe, P., Roberts, V. A., Osguthorpe, D. J., Wolff, J., Genest, M., and Hagler, A. T. (1988) *Proteins: Struct., Funct., Genet. 4*, 31−47.
50. Hagler, A. T., Dauber, P., and Lifson, S. (1979) *J. Am. Chem. Soc. 101*, 5131−5141.
51. Hagler, A. T., Lifson, S., and Dauber, P. (1979) *J. Am. Chem. Soc. 101*, 5122−5130.
52. Lifson, S., Hagler, A. T., and Dauber, P. (1979) *J. Am. Chem. Soc. 101*, 5111−5121.
53. van Gunsteren, W. F., and Mark, A. E. (1992) *Eur. J. Biochem. 204*, 947−961.
54. Berendsen, H. J. C., Postma, J. P. M., van Gunsteren, W. F., DiNola, A., and Haak, J. R. (1984) *J. Chem. Phys. 81*, 3684−3690.
55. Doucet, J. P. and Weber, J. (1996) *Computer-Aided Molecular Design: Theory & Applications*, Academic Press, Inc, San Diego, CA.
56. Lee, B., and Richards, F. M. (1971) *J. Mol. Biol. 55*, 379−400.
57. Hubbard, S. J., and Thornton, J. M. (1993) NACCESS, Department of Biochemistry and Molecular Biology, University College, London.
58. Desmarais, S., and Ramachandran, C. (1995) (Unpublished results).
59. Prinz, H., and Striessnig, J. (1993) *J. Biol. Chem. 268*, 18580−18585.
60. Deleted in proof.
61. Mikol, V., Baumann, G., Zurini, M. G. M., and Hommel, U. (1995) *J. Mol. Biol. 254*, 86−95.

62. Chen, L., Wu, L., Otaka, A., Smyth, M. S., Roller, P. P., Burke, T. R., Jr., Hertog, J. D., and Zhang, Z.-Y. (1995) *Biochem. Biophys. Res. Commun. 216*, 976−984.
63. Maclean, D., Sefler, A. M., Zhu, G., Decker, S. J., Saltiel, A. R., Singh, J., McNamara, D., Dobrusin, E. M., and Sawyer, T. K. (1995) *Protein Sci. 4*, 13−20.
64. Zhang, Z.-Y., Maclean, D., McNamara, D. J., Sawyer, T. K., and Dixon, J. E. (1994) *Biochemistry 33*, 2285−2290.
65. Zhang, Z.-Y., Thieme-Sefler, A. M., Maclean, D., McNamara, D. J., Dobrusin, E. M., Sawyer, T. K., and Dixon, J. E. (1993) *Proc. Natl. Acad. Sci. U.S.A. 90*, 4446−4450.
66. Singh, J., and Thornton, J. M. (1992) *Atlas of Protein Side-Chain Interactions*, Oxford University Press, New York.
67. Burke, T. R., Jr., Ye, B., Yan, X., Wang, S., Jia, Z., Chen, L., Zhang, Z.-Y., and Barford, D. (1996) *Biochemistry 35*, 15989−15996.
68. Blokzijl, W., and Engberts, J. B. F. N. (1993) *Angew. Chem., Int. Ed. Engl. 1993*, 1545−1579.
69. Krystek, S., Stouch, T., and Novotny, J. (1993) *J. Mol. Biol. 234*, 661−679.
70. Pannifer, A. D. B., Flint, A. J., Tonks, N. K., and Barford, D. (1998) *J. Biol. Chem. 273*, 10454−10462.
71. Burley, S. K., and Petsko, G. A. (1986) *FEBS Lett. 203*, 139−143.
72. Ma, J. C., and Dougherty, D. A. (1997) *Chem. Rev. 97*, 1303−1324.
73. Burley, S. K., and Petsko, G. A. (1985) *Science 229*, 23−28.
74. Singh, J., and Thornton, J. M. (1985) *FEBS Lett. 191*, 1−6.
75. Hunter, C. A., and Sanders, J. K. M. (1990) *J. Am. Chem. Soc. 112*, 5525−5534.
76. Hunter, C. A., Singh, J., and Thornton, J. M. (1991) *J. Mol. Biol. 218*, 837−846.
77. Jorgensen, W. L., and Severance, D. L. (1990) *J. Am. Chem. Soc. 112*, 4768−4774.
78. Borwick, S. J., Howard, J. A. K., Lehnmann, C. W., and O'Hagan, D. (1997) *Acta Crystallogr. C53*, 124−126.
79. Howard, J. A. K., Hoy, V. J., O'Hagan, D., and Smith, G. T. (1996) *Tetrahedron 5*, 12613−12622.
80. Wiley, R. A., and Rich, D. H. (1993) *Med. Res. Rev. 13*, 327−384.
81. Puius, Y. A., Zhao, Y., Lawrence, D. S., Almo, S. A., and Zhang, Z.-Y. (1997) *Proc. Natl. Acad. Sci. U.S.A. 94*, 13420−13425.
82. Sheinerman, F. B. and Brooks, C. L. I. (1997) *Proteins: Struct., Funct., Genet. 29*, 193−202.
83. Barford, D., Flint, A. J., and Tonks, N. K. (1994) *Science 263*, 1397−1404.
84. Daggett, V., and Levitt, M. (1993) *Annu. Rev. Biophys. Biomol. Struct. 22*, 353−380.
85. Siligardi, G., and Drake, A. F. (1995) *Biopolymers 37*, 281−292.
86. Stanfield, R. L., and Wilson, I. A. (1995) *Curr. Opin. Struct. Biol. 5*, 103−113.
87. Wlodawer, A., and Erickson, J. W. (1993) *Biochemistry 62*, 543−585.
88. Meek, T. D. (1992) *J. Enzyme Inhib. 6*, 65−98.
89. Stern, L. J., Brown, J. H., Jardetzky, T. S., Gora, J. C., Urban, R. G., Strominger, J. L., and Wiley, D. C. (1994) *Nature 368*, 215−221.
90. Young, A. C. M., Zhang, W., Sacchettini, J. C., and Nathenson, S. G. (1994) *Cell 76*, 39−50.
91. Waksman, G., Kominos, D., Roberston, S. C., Pant, N., Baltimore, D., Birge, R. B., Cowburn, D., Hanafusa, H., Mayer, B. J., and Overduin, M. (1992) *Nature 358*, 646−653.
92. Waksman, G., Shoelson, S. E., Pant, N., Cowburn, D., and Kuriyan, J. (1993) *Cell 72*, 779−790.
93. Babine, R. E., and Bender, S. L. (1997) *Chem. Rev. 97*, 1359−1472.
94. Zhang, Z.-Y., Thieme-Sefler, A. M., Maclean, D., Roeske, R., and Dixon, J. E. (1993) *Anal. Biochem. 211*, 7−15.
95. Burley, S. K., and Petsko, G. A. (1988) *Adv. Protein Chem. 39*, 125−189.
96. Baker, E. N., and Hubbard, R. E. (1984) *Prog. Biophys. Mol. Biol. 44*, 97−179.
97. McDonald, I. K., and Thornton, J. M. (1994) *J. Mol. Biol. 238*, 777−793.
98. Kabsch, W., and Sander, C. (1983) *Biopolymers 22*, 2577−2637.

BI9825450